

RESEARCH ARTICLE

POLYMER
ENGINEERING
AND SCIENCE

WILEY

Pressure-dependent heat transfer coefficient measurement for thermoplastic melts

Béla Zink¹ | József Gábor Kovács^{1,2}

¹Department of Polymer Engineering,
Faculty of Mechanical Engineering,
Budapest University of Technology and
Economics, Budapest, Hungary

²MTA-BME Lendület Lightweight
Polymer Composites Research Group,
Budapest, Hungary

Correspondence

József Gábor Kovács, MTA-BME Lendület
Lightweight Polymer Composites
Research Group, Műegyetem rkp. 3.,
H-1111 Budapest, Hungary.
Email: kovacs@pt.bme.hu

Funding information

National Research, Development and
Innovation Office, Grant/Award Numbers:
2017-2.3.7-TET-IN-2017-00049,
2018-1.3.1-VKE-2018-00001,
2019-1.1.1-PIACI-KFI-2019-00205; NKFIH
Hungary; BME NC, Grant/Award
Number: TKP2020

Abstract

A common calculation error of thermal processes in injection molding simulation programs is caused by the inadequate description of the heat transfer between the polymer melt and the wall of the mold. No correct description of the effect of pressure on the heat transfer coefficient is available for the numerical calculations of injection molding yet. During the injection molding cycle, the pressure of the melt can vary from atmospheric pressure to thousands of bars. When such a high pressure is applied, the heat transfer coefficient can change several orders of magnitude. To calculate heat removal accurately, we developed a novel measuring method and based on the measurement data, we created a model that describes the heat transfer coefficient as a function of pressure and temperature. Calculated maximal heat transfer coefficients vary between 250 and 800 W/(mK) at the pressure of 500 bar. The pressure dependence of the heat transfer coefficient can be described with a sigmoid function. The heat transfer coefficient increases as the temperature difference between mold and melt increases and as pressure increases. We determined measurement error and found it to be less than 5%.

KEYWORDS

melt, modeling, thermal properties, thermoplastics

1 | INTRODUCTION

When thermoplastic polymers are injection molded, the heat is taken into the mold with the hot melt. The heat is transferred to the mold via heat transfer from where it is carried by heat conduction to nearby mold parts and the cooling liquid. As a result, the more accurate the heat transfer coefficient between the wall of the mold and the polymer melt is, the more accurate the numerical calculations of heat transport are. The temperature distribution of the mold, which is obtained by the heat transfer

calculations, is an input parameter of filling and deformation calculations and so it determines several factors including the filling pattern, pressure distribution, and warping; therefore, the accuracy of the calculation of thermal processes is of paramount importance. The heat transfer coefficient between the melt and the mold wall depends on numerous parameters, including pressure, the temperature difference, the viscosity of the melt, and the surface roughness of the mold, so it is very difficult to calculate or approximate it. Simulation programs, such as Modflow, Sigmasoft, and Cadmould, use a constant heat

This is an open access article under the terms of the Creative Commons Attribution-NonCommercial-NoDerivs License, which permits use and distribution in any medium, provided the original work is properly cited, the use is non-commercial and no modifications or adaptations are made.

© 2022 The Authors. *Polymer Engineering & Science* published by Wiley Periodicals LLC on behalf of Society of Plastics Engineers.

transfer coefficient and do not consider its dependence on pressure, temperature difference, and surface roughness. They divide the injection molding process into three sections, injection, holding, and residual cooling, and approximate the heat transfer coefficient with constant values. Moldex 3D is the only program capable of approximating the heat transfer coefficient better; it determines the heat transfer coefficient from the Nusselt equation and, therefore, considers the geometry of the part.

Yu et al.^[1] were the first to consider the effect of the heat transfer coefficient between the polymer melt and the wall of the mold in numerical calculations and found that the calculation of cooling time greatly depends on the accuracy of the heat transfer coefficient. Young^[2] found that the maximum flow path largely depends on the heat transfer coefficient in the 1000–10,000 W/m²K range. Otmani et al.^[3] state that the heat transfer coefficient is a key input parameter for numerical calculations. Researchers have focused on determining the heat transfer coefficient, both experimentally and numerically.^[4–17] Bendada et al.^[4] performed experiments and found it to be 1250–5000 W/(m²K). Masse et al.^[5] report a similar heat transfer coefficient; it varied between 1000 and 5000 W/(m²K) depending on cycle time. Beilharz et al.^[6] found that the heat transfer coefficient is below 250 W/(m²K) at room temperature but can reach up to 100,000 W/(m²K) depending on the hardness of tool steel. Goff et al.^[7] found that the heat transfer coefficient to be between 200 and 1000 W/(m²K). Brunotte^[8] stated that the heat transfer coefficient also depends on the type of the material; for polypropylene, it is 500–600 W/(m²K), and for polycarbonate, it is 400–600 W/(m²K). Liu and Gehde^[9] calculated a higher heat transfer coefficient than Masse et al.^[5]; according to his experiments, the heat transfer coefficient varies between 18,000 and 36,000 W/(m²K). Dawson et al.^[10] calculated a heat transfer coefficient of 5000–7500 W/(m²K). Nguyen-Chung et al.^[11–13] varied the heat transfer coefficient in numerical calculations to calibrate the results to temperature measurements—his results were between 0 and 30,000 W/(m²K). It is evident that the research results differ; the heat transfer coefficient varies in a wide range based on the measurement method, the properties of the material, the processing parameters, and surface roughness. Several researchers^[14–16] have shown that higher surface roughness increases heat transfer, but only if the viscosity of the polymer is low enough to follow the contour of the surface. Otsuka et al.,^[17] however, pointed out that if surface roughness is increased, air gaps form, which increases thermal resistance, thus the achievable maximum flow path during injection. Several other researchers investigated the heat transfer coefficient between injection molds and the polymer melt and built

models.^[18,19] Some researchers focused on the heat transfer coefficient in microinjection molding^[20,21] and microfoam^[22] injection molding. Researchers usually examined parameters that only affect heat transfer indirectly (surface roughness, injection pressure, etc.). However, the heat transfer coefficient is also directly influenced by cavity pressure and temperature difference. The authors did not find a relationship between the measured parameters and the heat transfer coefficient.

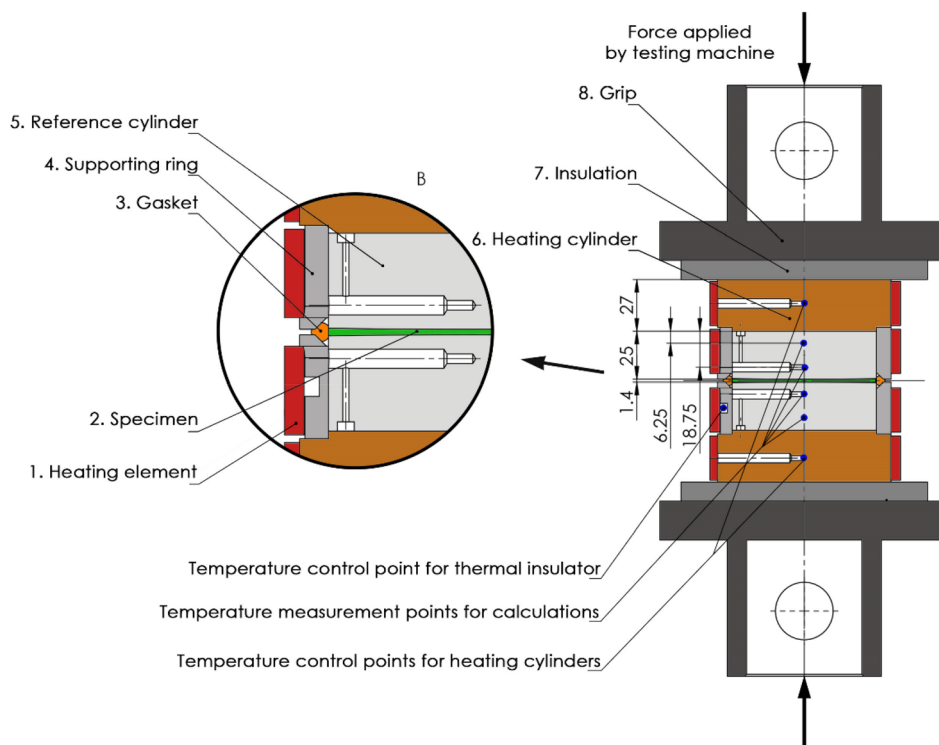
We developed a new measurement method and a new device to determine the heat transfer coefficient between the melt and the mold wall as a function of pressure and temperature difference, and created a formula from the heat transfer coefficients calculated from the measurement results. With the formula, the heat transfer coefficient can be calculated from the temperature difference and pressure.

2 | DEVELOPMENT OF THE METHOD

2.1 | Equipment and measurement method

The equipment (Figure 1) can determine the heat transfer coefficient/thermal contact resistance on the surface of the sample between the two reference cylinders. The specimen (Figure 1, Part 2) used for the tests had a shape of a disc with a diameter of 75 mm and a thickness of 2 mm. The 1.2344 steel reference cylinders are 75 mm in diameter and 25 mm in height (Figure 1, Part 5). The surface of cylinders on the specimen side has a radius of R2500 mm to ensure there is no trapped air between the reference cylinder and the specimen. The three temperature measurement points in each reference cylinder were machined at equal differences from each other and also from the surface (6.25 mm). The holes (bored in the side of the reference cylinders) used to fit the temperature measurement sensors are rotated by 12° from each other. The ends of the holes are in the centerline of the reference cylinder. The reference cylinders are held concentric by the support rings (Figure 1, Part 4), and these transfer the load to the gasket (Figure 1, Part 3), which insulates the specimen from the environment. The temperature sensors for temperature control were inserted in the lateral, curved surface of the support rings. These temperature sensors are used to control the temperature of the cylindrical heating elements. The heating cylinders (Figure 1, Part 6) are inserted between the reference cylinders and the grips (Figure 1, Part 8). The heating cylinders are made from the Ampcoloy 88 copper alloy. Its high thermal conductivity ensures an even temperature distribution on the

FIGURE 1 The schematic illustration of the equipment used for the measurement of the heat transfer coefficient



heating surface. Heating is ensured by the heating elements on the lateral surface of the heating plates (Figure 1, Part 1), with a power of 250 W each. The signal of the temperature sensors in the holes of the copper cylinders is used to control the heating of the heating elements. The sensors were M 222 PT 1000 (Heraeus Group) platinum temperature sensors, which have an accuracy of 0.15°C in the temperature range where we used them. We put granite plates (Figure 1, Part 7) between the pressing plates and the heating plates for heat insulation because the thermal conductivity of granite is several orders of magnitude lower^[23] than that of copper or steel, but its compressive strength^[24] is higher than the compressive strength needed during the tests (22 MPa). On the outer curved surface of the support rings, there are two more heating elements with which the temperature of the support rings can be set. This way, heat transport to the environment is reduced and so it does not influence the measurement results in the central line of the cylinders. The temperature of the support rings was set to match the measured average heating element temperature of the relevant reference cylinders when only the two other heating elements were turned on. Surface temperature was measured with a Flir A325SC infrared camera in the area cut out for the cables of the platinum temperature sensors. We applied the pressure on the specimen with a Zwick Z250 (Zwick Roell Group) universal tester. The greatest force used was 220 kN, which meant 500 bar considering the 75 mm diameter of the specimen.

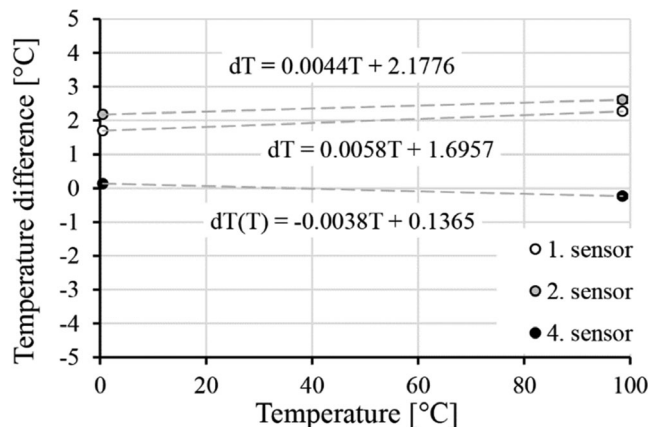


FIGURE 2 Calibration curves of the temperature sensors

2.2 | Calibration and the mathematical model

The heat provided by the heating element provides a heat flux from the hotter side to the colder side. When equilibrium is reached, the time derivative of the heat flux is zero so the thermal resistance can be calculated from the measured temperatures. The temperature of the reference cylinders was measured in three points each. To improve accuracy, we calibrated Sensors 1, 2, and 4 to Sensor 3 at 0.5 and 98.5°C (Figure 2). The values of Sensor 4 are different from the values of Sensors 1 and 2 because two

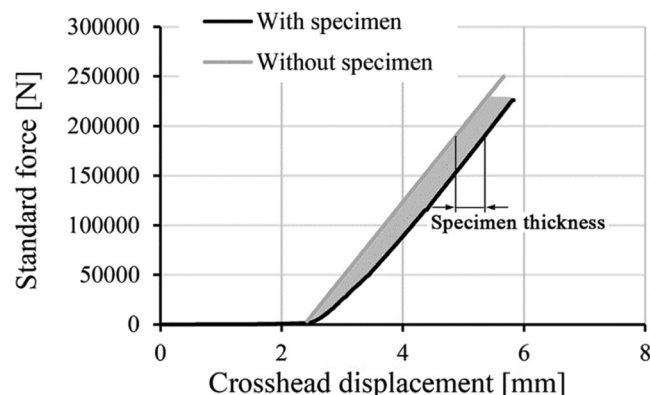


FIGURE 3 The thickness of the specimen determined from crosshead displacement

analog-digital converters were used to process the signals. Therefore, there is a basic signal difference between Sensors 1 and 2, and Sensors 3 and 4.

The thickness of the specimen was determined from the crosshead displacement of the tensile tester. It decreased with increasing pressure. The accuracy of measurement is also affected by the deformation of the tensile tester equipment, so we determined the deformation of the equipment as a function of pressure without the specimen (Figure 3).

The thickness of the specimen is the difference of the curve measured during the test and the calibration curve measured without the specimen. The curve only starts to go up after a crosshead displacement of 2.5 mm, due to fitting gaps; we determined the exact location of this point by examining the slope change of the curve.

The heat transfer coefficient was determined with the following neglects:

- The heat transfer coefficient is the same on both sides of the sample.
- Heat is transferred only vertically, from the hotter reference cylinder to the colder reference cylinder; heat transferred to the insulation is neglected.
- The thermal conductivity of the sample is considered constant in the measurement temperature range.

After equilibrium is reached, the heat flux is constant in time, and the slopes of the temperature curves of the reference cylinders are constant. Therefore, the measured temperature values can be extrapolated onto the surface. The Fourier equation yields the heat flux through the reference cylinders and the sample. If there is no heat transfer to the environment, the heat flux through the reference cylinders and the heat flux through the specimen are equal, so Equation (1) is valid for the sample:

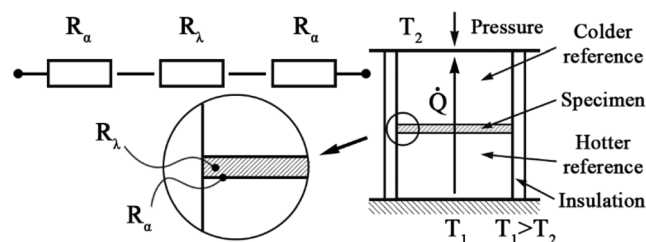


FIGURE 4 The model of the thermal resistance of the measurement layout

$$\dot{Q} \cdot R_m = \Delta T_{\text{ref,surface}}, \quad (1)$$

where \dot{Q} is the heat flux through the sample, R_m is the thermal resistance of the sample, $\Delta T_{\text{ref,surface}}$ is the difference between the temperatures of the surfaces (which contact the specimen) of the colder and warmer reference cylinders. The thermal resistance of the sample can be calculated from heat conduction and heat transfer on the two sides (Figure 4); therefore, thermal resistance according to Equation (2) is:

$$R_m = \frac{1}{A_s \cdot \alpha_1} + \frac{\delta_{\text{sample}}}{A_{\text{cs}} \cdot \lambda_{\text{sample}}} + \frac{1}{A_s \cdot \alpha_2} (\alpha_1 = \alpha_2), \quad (2)$$

where α_1 and α_2 are the heat transfer coefficients on the hotter and colder surface, δ_{sample} is the thickness of the sample, λ_{sample} is the thermal conductivity of the sample, A_{cs} is the cross-sectional area of the sample, which is the same as that of the reference cylinders, and A_s is the area of the reference cylinders in connection with the sample. We set the heat conductivity of the specimen from the database of the Autodesk Moldflow Insight program. Since thermal conductivity is temperature dependent, we used the mean temperature of the specimen to determine its thermal conductivity:

$$T_{\text{sample}} = \frac{T_{\text{ref,surf,hot}} + T_{\text{ref,surf,cold}}}{2}, \quad (3)$$

where $T_{\text{ref,surf,hot}}$ and $T_{\text{ref,surf,cold}}$ are the surface temperatures of the hotter and the colder reference cylinder, and T_{sample} is the mean temperature of the specimen.

The heat transfer coefficient (4) can be calculated from Equations (1) and (2) with the assumption that the heat transfer coefficient is the same on both sides of the sample:

$$\frac{\Delta T_{\text{ref,surface}}}{\dot{Q}} = R_m = \frac{\delta_{\text{sample}}}{A_{\text{cs}} \cdot \lambda_{\text{sample}}} + \frac{2}{\alpha \cdot A_s} (\alpha_1 = \alpha_2 = \alpha), \quad (4)$$

where α is the average heat transfer coefficient on the two sides of the specimen. Heat flux can be calculated with the use of the thermal properties and temperatures of the reference cylinders (5):

$$\dot{Q} = A_{cs} \cdot \lambda_{ref} \cdot \frac{\Delta T_{ref}}{h_{ref}}, \quad (5)$$

where λ_{ref} is the thermal conductivity of the reference cylinders, h_{ref} is the height of the reference cylinders, ΔT_{ref} is the temperature difference between the top and bottom of the reference cylinders. After rearranging, the heat transfer coefficient can be calculated with Equation (6) from the measured temperature and specimen thickness data:

$$\alpha = \frac{2 \cdot A_{cs} \cdot \lambda_{ref} \cdot \frac{\Delta T_{ref}}{h_{ref}} \cdot \lambda_{sample}}{\lambda_{sample} \cdot A_s \cdot \Delta T_{ref,surface} - A_s \cdot \lambda_{ref} \cdot \frac{\Delta T_{ref}}{h_{ref}} \cdot \delta_{sample}}. \quad (6)$$

2.3 | Materials and thermal properties

Injection molded plates, produced from Terluran GP-35 (INEOS Styrolution) acrylonitrile butadiene were used for the heat transfer coefficient measurements. Specimens with a diameter of 75 mm and a thickness of 2 mm were cut from the original $80 \times 80 \times 2$ mm plates. Figure 5 shows the temperature-dependent thermal conductivity of the material.

The main parts of the equipment, such as the reference cylinders, support ring, and so on, were made from 1.2344 steel (Table 1). The heating plates are from the Ampcoloy 88 copper alloy due to its much higher thermal conductivity. In our calculations, we considered the

changing thermal conductivity of the reference cylinders (Figure 6).

3 | RESULTS AND DISCUSSION

3.1 | Determining the heat transfer coefficient

We calculated the heat transfer coefficient at 25, 50, 100, 250, and 500 bar and at a temperature difference of 5, 10, 25, 50, and 70°C. The temperature differences are measured between the reference cylinders, which we set with the heating elements. The colder side was set to 30°C for the temperature difference of 5°C (35°C for the hot side) and 10°C (40°C for the hot side). For a temperature difference of 25 and 50°C, the temperature of the colder side rose to 40°C due to the heat transfer, therefore, we used this temperature for the colder side (the temperature of the hot side was set to 65 and 75°C, respectively). At a temperature difference of 70°C, the temperature of the colder side was 70°C (140°C for the hot side). The transition temperature of the material is

TABLE 1 The main properties of the materials used for the equipment

	1.2344 steel	Ampcoloy 88
Density (kg/m ³)	7800	8750
Tensile strength (MPa)	1600	890
Young's modulus (GPa)	215	130
Thermal conductivity coefficient (W/[mK])	25.6	230
Specific heat capacity (J/[kg K])	460	420

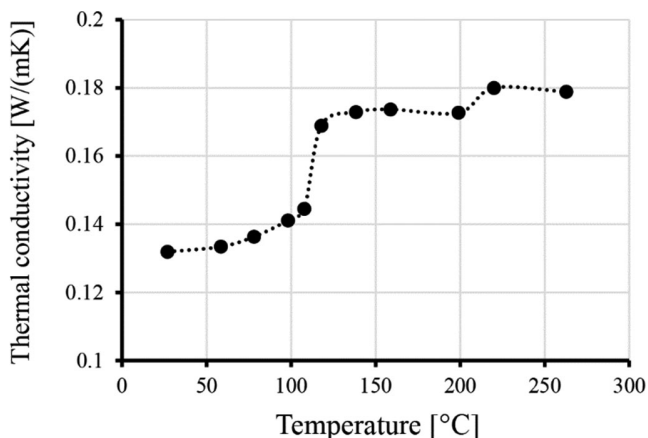


FIGURE 5 Thermal conductivity of Terluran GP-35

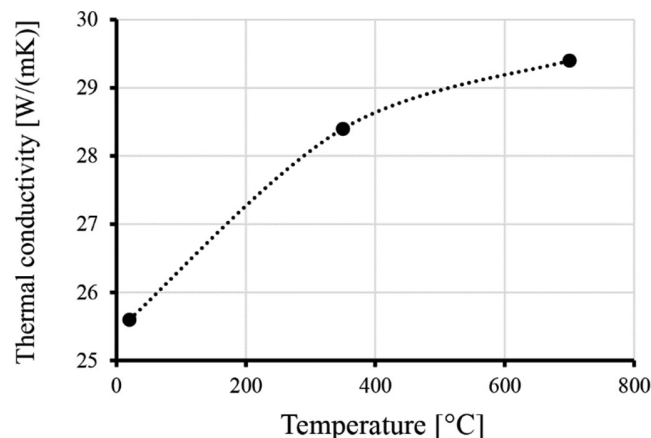


FIGURE 6 Thermal conductivity of 1.2344 steel

94°C, therefore, we performed a measurement where one side of the reference cylinders was 160°C, and the other side was 200°C, so the material was certain to melt. We inserted the specimen and the gasket into the equipment after the heating plates and the reference cylinders were heated up. We waited for the temperature equilibrium. We set the heating of the lateral surface of the cylinders to be 0.2–0.4°C higher than the temperature measured in the reference cylinders, because this way less heat was transferred to the environment, but it did not affect the temperature of the sensors. Then we started the test and created the pressure on the specimen with the tensile tester, and monitored the temperature of the reference cylinders until the temperature equilibrium was reached. Then we started measuring the temperature with a sampling rate of 6 per second. We used the average of at least 100 measured values to calculate the heat transfer coefficient in each case.

Using Equation (6), we calculated the heat transfer coefficient for the temperature differences of 5, 10, 50, and 70°C (Figure 7). As the pressure and temperature difference increases, the heat transfer coefficient also increases, which means the function describing the heat transfer coefficient must be continuous and strictly increasing in the range of $[0 - \infty]$, where the coefficient can be interpreted. Furthermore, the function must be bounded, because the maximum of the

heat transfer coefficient is reached at a theoretical infinite pressure. Therefore, we described the pressure dependence of the heat transfer coefficient by fitting a sigmoidal function on the heat transfer values calculated from the measured data with Equation (6). Based on the preliminary testing of several basic sigmoidal functions, for example, Weibull, Hill, Boltzmann, BoltzV, and so on, Equation (7) was chosen for its adequate model fit. Table 2 contains the fitting parameters and the sum of the fitting errors^[25]:

$$\alpha(p) = \alpha_0 + \alpha'_\infty \cdot \tanh\left(\frac{k}{2}p^l\right), \quad 0 \leq p \leq 500, \quad (7)$$

where α_0 is the heat transfer coefficient at a pressure of zero bar, α'_∞ is the asymptotic heat transfer coefficient, p is the pressure on the specimen, and k and l are fitting constants. We assumed that during injection molding, the pressure between the polymer and the mold cannot be zero. During filling and holding, where there can be melt next to the mold wall, the pressure is definitely larger than zero. When the pressure can decrease to zero, the product must be in the residual cooling phase, where the melt state is impossible. Therefore, we assumed that when the product is cooling and shrinking, and pressure is zero, the heat transfer coefficient is 0 W/(m²K)

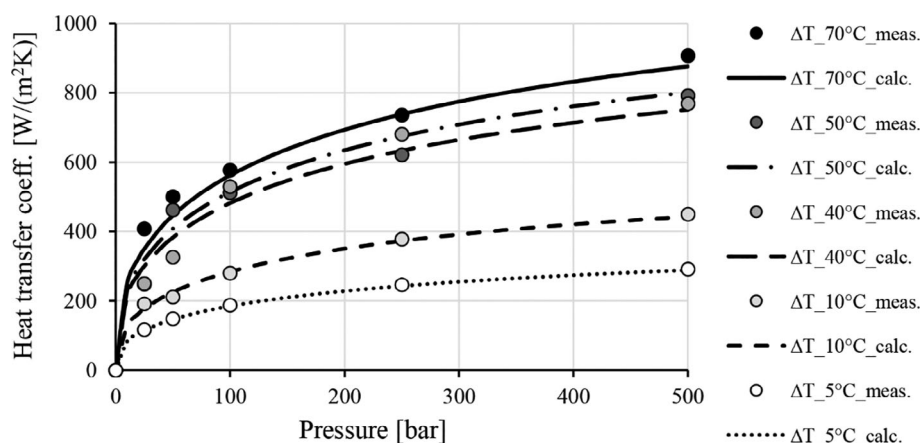


FIGURE 7 The calculated heat transfer coefficients and the fitted curves as a function of pressure and temperature difference

	Temperature difference (°C)				
	5	10	40	50	70
α'_∞ (W/[m ² K])	396.5	604.4	1035.81	1067.3	1222.6
k [1/bar]	0.188				
l [–]	0.377				
α_0 (W/[m ² K])	0				
SE (W/[m ² K])	12.85	6.15	13.87	13.3	10.82
Adjusted R^2 (–)	0.9531	0.9360	0.9740	0.9722	0.9925

TABLE 2 The parameters of fitting

($\alpha_0 = 0$), because in this case, the surface of the part is no longer in contact with the mold wall. The measured heat transfer coefficients at 500 bar are similar to those found

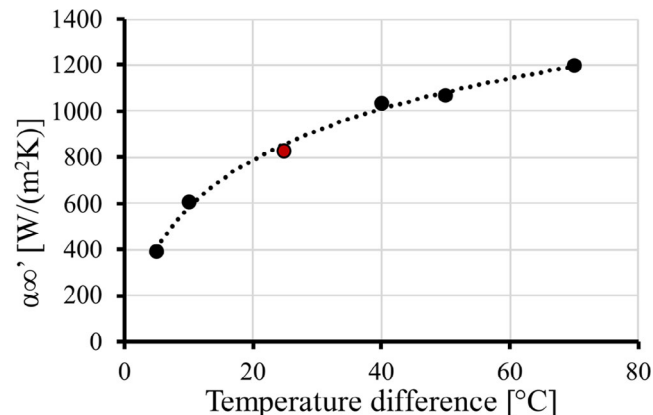


FIGURE 8 The α_{∞}' asymptotic heat transfer coefficient as a function of temperature difference; the control measurement ($\Delta T = 25^{\circ}\text{C}$) is marked by red

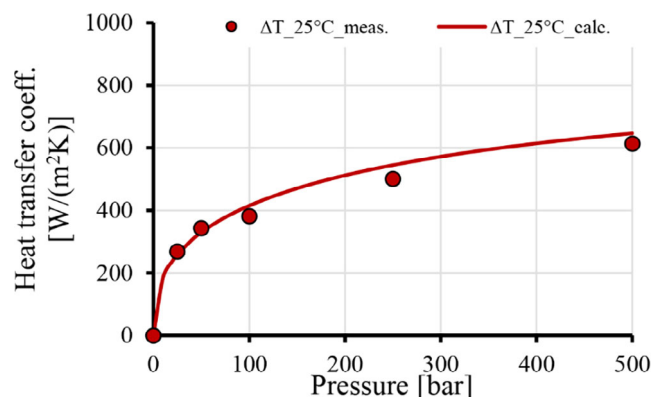


FIGURE 9 The heat transfer coefficients calculated for a temperature difference of 25°C , and the heat transfer coefficients calculated with the model that takes into account pressure and temperature difference

in other publications,^[7,8] although a wide range of heat transfer coefficients are reported in the literature.

If α_{∞}' , the asymptotic heat transfer coefficient is plotted as a function of temperature difference, the temperature dependence of the α_{∞}' parameter can be calculated (Figure 8). If the temperature difference between the melt and the mold is 0°C , there is no heat transfer. If the temperature difference increases to a theoretical infinite, the heat transfer is also infinite. The aim was to find the simplest function for the regression model which also satisfies the initial conditions, therefore, we tested simple functions (linear, exponential, logarithmic, etc.). The best fit for the regression model in the range of the measurement data was found with a logarithmic function. The equation of the curve fitted on the parameters is^[25]:

$$\alpha_{\infty}'(\Delta T) = C_1 \cdot \ln\left(\frac{\Delta T + C_2}{C_2}\right), \quad (8)$$

where $C_1 = 345.3$ (W/[m²K]) and $C_2 = 2.28$ (K) are the temperature difference constants of the heat transfer coefficient. The adjusted R^2 of the fitting is .994.

If Equation (8) is substituted back into Equation (7), the pressure and temperature difference-dependent equation of the heat transfer coefficient can be obtained (9):

$$\alpha(p, \Delta T) = C_1 \cdot \ln\left(\frac{\Delta T + C_2}{C_2}\right) \cdot \tanh\left(\frac{k}{2} p^l\right), \quad 0 \leq p \leq 500. \quad (9)$$

To validate the proposed model, we performed another test with a temperature difference of 25°C , calculated the heat transfer coefficient with Equation (6) as a function of pressure, and fitted a curve on the measured points with Equation (7) (Figure 9). The α_{∞}' parameter was 836.8 W/(m²K) with the Levenberg–Marquardt fitting, which is less than a 4% difference compared to the α_{∞}' parameter calculated with Equation (8) (Figure 8).

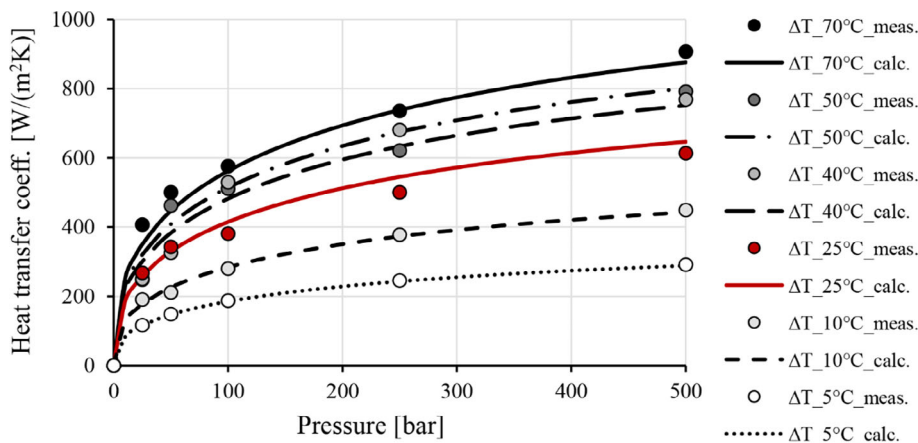


FIGURE 10 The heat transfer coefficients calculated for temperature differences of 5, 10, 25, 50, and 70°C , and the curves fitted to the measured points

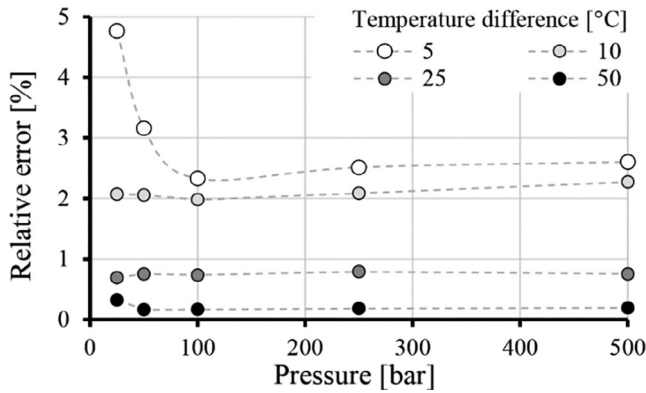


FIGURE 11 Relative error as a function of pressure

Figure 10 shows the heat transfer coefficients supplemented with the measurement results with a temperature difference of 25°C and the pressure-dependent heat transfer coefficients calculated with Equation (9).

The sign of accidental errors can be positive or negative. They cannot be eliminated, and only their average effect can be taken into account.

The sign and magnitude of regular errors do not change if the test conditions are the same. The error can be estimated if the error of the measuring equipment is known. In our tests, there can be regular errors in the measurement of temperature and specimen thickness. The error of the temperature sensors is 0.15°C in the temperature range we used; assuming a worst-case scenario, we calculated with a temperature difference error of 0.3°C. We measured the thickness of the specimen using the crosshead displacement of the tensile tester. The accuracy of its crosshead displacement is 2 μm; therefore, the measurement error is 2 μm.

In our tests, the quadratic absolute error of the heat transfer coefficient can be given with Equation (10):

$$\delta\alpha = \sqrt{\sum_{i=1}^n \left(\delta X_i \cdot \frac{\partial \alpha}{\partial X_i} \right)^2} = \sqrt{\left(\delta\Delta T_{\text{ref}} \cdot \frac{\partial \alpha}{\partial \Delta T_{\text{ref}}} \right)^2 + \left(\delta\Delta T_{\text{ref,surface}} \cdot \frac{\partial \alpha}{\partial \Delta T_{\text{ref,surface}}} \right)^2 + \left(\delta\delta_{\text{sample}} \cdot \frac{\partial \alpha}{\partial \delta_{\text{sample}}} \right)^2}, \quad (10)$$

3.2 | Calculating measurement error

Measurement error is the sum of regular, accidental, and statistical errors. This article focuses on regular and accidental errors. We estimated the differences caused by regular errors. The following factors may cause unexpected errors:

- The fluctuation of ambient temperature.
- Incorrect assembly, for example, sensor positions are changed or reference cylinders are turned.
- The air gap between the specimen and the reference cylinders.
- Fitting clearances.
- The error of temperature control.

where $\delta\alpha$ is the absolute error of the heat transfer coefficient, δX_i is the error of the measured quantities, $\delta\Delta T_{\text{ref}}$ is the measurement error of the temperatures of the reference cylinders (0.3°C), $\delta\Delta T_{\text{ref,surface}}$ is the measurement error of the temperature of the surface of the reference cylinders (0.3°C) and $\delta\delta_{\text{sample}}$ is the measurement error of the thickness of the specimen (0.000002 m). After performing partial derivation on the equation of the heat transfer coefficient, we get Equations (11–13):

$$\frac{\partial \alpha}{\partial \Delta T_{\text{ref}}} = \frac{2 \cdot \lambda_{\text{sample}}^2 \cdot \lambda_{\text{ref}} \cdot h_{\text{ref}} \cdot \Delta T_{\text{ref}} \cdot A_{\text{cs}}}{A_{\text{s}} (\lambda_{\text{sample}} \cdot h_{\text{ref}} \cdot \Delta T_{\text{ref,surface}} - \lambda_{\text{ref}} \cdot \delta_{\text{sample}} \cdot \Delta T_{\text{ref}})^2}, \quad (11)$$

$$\frac{\partial \alpha}{\partial \Delta T_{\text{ref, felület}}} = \frac{2 \cdot \lambda_{\text{sample}}^2 \cdot \lambda_{\text{ref}} \cdot h_{\text{ref}} \cdot \Delta T_{\text{ref}} \cdot A_{\text{cs}}}{A_{\text{s}} (\delta_{\text{sample}} \cdot h_{\text{ref}} \cdot \Delta T_{\text{ref}} - \lambda_{\text{ref}} \cdot \lambda_{\text{sample}} \cdot \Delta T_{\text{ref,surface}})^2}, \quad (12)$$

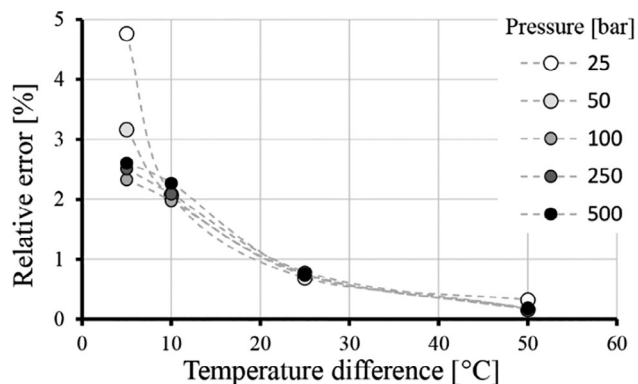


FIGURE 12 Relative error as a function of temperature difference

TABLE 3 The relative error for all pressure and temperature difference values used

		Temperature difference (°C)				
		5	10	25	50	70
Pressure (bar)	25	4.77%	2.07%	0.69%	0.32%	0.21%
	50	3.16%	2.06%	0.75%	0.16%	0.24%
	100	2.33%	1.98%	0.74%	0.17%	0.24%
	250	2.51%	2.09%	0.79%	0.18%	0.24%
	500	2.74%	2.27%	0.75%	0.19%	0.19%

$$\frac{\partial \alpha}{\partial \delta_{\text{minta}}} = \frac{2 \cdot \lambda_{\text{ref}}^2 \cdot \lambda_{\text{sample}} \cdot \Delta T_{\text{ref}}^2 \cdot A_{\text{cs}}}{A_{\text{s}} (\lambda_{\text{sample}} \cdot h_{\text{ref}} \cdot \Delta T_{\text{ref, surface}} - \lambda_{\text{ref}} \cdot \delta_{\text{sample}} \cdot \Delta T_{\text{ref}})^2} \quad (13)$$

The relative error is the quotient of Equations (9) and (10):

$$\frac{\delta \alpha}{\alpha} = \sqrt{\frac{(\delta \Delta T_{\text{ref}} \cdot \frac{\partial \alpha}{\partial \Delta T_{\text{ref}}})^2 + (\delta \Delta T_{\text{ref, surface}} \cdot \frac{\partial \alpha}{\partial \Delta T_{\text{ref, surface}}})^2 + (\delta \delta_{\text{sample}} \cdot \frac{\partial \alpha}{\partial \delta_{\text{sample}}})^2}{\alpha^2}} \quad (14)$$

The error is greatest when the temperature difference and the pressure are smallest because the error of the temperature sensors influences the measurement results most when the temperature difference is smallest. Relative error as a function of pressure (Figure 11) only changes considerably when the temperature difference is 5°C; otherwise, the change is negligible. As temperature increases, the error decreases exponentially (Figure 12). The error is most significant when the temperature difference is 5°C, and the pressure is 25 bar (Table 3), but even then it is less than 5%.

4 | CONCLUSION

We developed a measurement method and a device to determine the heat transfer coefficient between the mold wall and the melt as a function of pressure and temperature difference. We compressed polymer specimens between two reference cylinders at a pressure of 25, 50, 100, 250 and 500 bar with a tensile tester. Using the measurement results, we calculated the heat transfer coefficient and made a formula with which the heat transfer coefficient can be calculated as a function of the pressure and the temperature difference. We performed additional measurements to check the accuracy of the formula and proved that the formula is correct. We also calculated the error of the method we developed.

ACKNOWLEDGMENTS

This work was supported by the National Research, Development and Innovation Office, Hungary (2019-1.1.1-PIACI-KFI-2019-00205, 2018-1.3.1-VKE-2018-00001, 2017-2.3.7-TÉT-IN-2017-00049). The research reported in this article was also supported by the BME NC TKP2020 grant of NKFIH Hungary.

NOMENCLATURE

A_{cs}	cross section of the specimen
A_{s}	surface of the reference cylinders in contact with the specimen
C_1	temperature difference constant of the heat transfer coefficient
C_2	temperature difference constant of the heat transfer coefficient
h_{ref}	height of the reference cylinders
k	curve fitting constant
l	fitting constant
p	pressure on the specimen
Q	heat flux going through the specimen
R_{m}	thermal resistance of the sample
ΔT_{ref}	thermal difference of the reference cylinders
$\Delta T_{\text{ref, surface}}$	temperature difference of the surfaces (which contact the specimen) of the colder and warmer reference cylinders
$T_{\text{ref, surf, cold}}$	surface temperature of the colder reference cylinder
$T_{\text{ref, surf, hot}}$	surface temperature of the warmer reference cylinder
T_{sample}	mean temperature of the specimen
α	the average heat transfer coefficient on the two sides of the specimen
α_0	heat transfer coefficient at 0 bar
α_1	heat transfer coefficient on the hotter surface
α_2	heat transfer coefficient on the colder surface
α'_{∞}	asymptotic heat transfer coefficient

$\delta\Delta T_{\text{ref}}$	temperature measurement error of the reference cylinders
$\delta\Delta T_{\text{ref, surface}}$	temperature measurement error on the surface of the reference cylinders
δ_{sample}	thickness of the sample
δXi	error of the measured quantities
$\delta\delta_{\text{sample}}$	measurement error of the thickness of the sample
λ_{ref}	thermal conductivity of the reference cylinders
λ_{sample}	thermal conductivity of the specimen

ORCID

Béla Zink  <https://orcid.org/0000-0002-7172-1484>

József Gábor Kovács  <https://orcid.org/0000-0002-7391-7085>

REFERENCES

- [1] C. J. Yu, J. E. Sunderland, C. Poli, *Polym. Eng. Sci.* **1990**, *30*, 1599.
- [2] W. B. Young, *Appl. Math. Model.* **2007**, *31*, 1798.
- [3] R. E. Otmani, M. Zinet, M. Boutaous, H. Benhadid, *J. Appl. Polym. Sci.* **2011**, *121*, 1579.
- [4] A. Bendada, A. Derdouri, M. Lamontagne, Y. Simard, *Appl. Therm. Eng.* **2004**, *24*, 2029.
- [5] H. Massé, É. Arquis, D. Delaunay, S. Quilliet, P. H. Le Bot, *Int. J. Heat Mass Transfer* **2004**, *47*, 2015.
- [6] F. Beilharz, K. Kouba, H. Blokland, P. Eyerer, presented at Polym. Process. Soc. Regional Meet., Gothenburg, **2007**. https://www.researchgate.net/publication/274072670_BEILHARZ_F_KOUBA_K_BLOKLAND_H_EYERER_P_Experimental_Investigation_of_friction_thermal_conductivity_and_heat_transfer_and_their_mathematical_description_for_the_thermoforming_process_simulation_Polymer
- [7] R. L. Goff, G. Poutot, D. Delaunay, R. Fulchiron, E. Koscher, *Int. J. Heat Mass Transfer* **2005**, *48*, 5417.
- [8] Brunotte, R.: *PhD Dissertation*, Technische Universität Chemnitz (Chemnitz, Germany) **2006**.
- [9] Y. Liu, M. Gehde, *Appl. Therm. Eng.* **2015**, *80*, 238.
- [10] A. Dawson, M. Rides, C. R. G. Allen, J. M. Urquhart, *Polym. Test.* **2008**, *27*, 555.
- [11] T. Nguyen-Chung, G. Jüttner, T. Pham, G. Mennig, M. Gehde, *Z. Kunststofftechnik* **2008**, *4*, 1.
- [12] T. Nguyen-Chung, G. Jüttner, C. Löser, T. Pham, M. Gehde, *Polym. Eng. Sci.* **2010**, *50*, 165.
- [13] T. Nguyen-Chung, C. Löser, G. Jüttner, M. Obadal, T. Pham, M. Gehde, *Z. Kunststofftechnik* **2011**, *7*, 86.
- [14] S. G. Kandlikar, S. Joshi, S. R. Tian, *Heat Transfer Eng.* **2003**, *24*, 4.
- [15] J. Koo, C. Kleinstreuer, *Int. J. Heat Mass Transfer* **2005**, *13*, 2625.
- [16] G. Croce, P. D. Agaro, *Superlattices Microstruct.* **2004**, *35*, 601.
- [17] M. Otsuka, A. Oyabe, H. Ito, *Polym. Eng. Sci.* **2011**, *51*, 1383.
- [18] B. Pignon, V. Sobotka, N. Boyard, D. Delaunay, *Int. J. Heat Mass Transfer* **2018**, *118*, 14.
- [19] J. G. Kovács, F. Szabó, N. K. Kovács, A. Suplicz, B. Zink, T. Tábi, H. Hargitai, *Appl. Therm. Eng.* **2015**, *85*, 44.
- [20] M. Babenko, J. Sweeney, P. Petkov, F. Lacan, S. Bigot, B. Whiteside, *Appl. Therm. Eng.* **2018**, *130*, 865.
- [21] J. Pina-Estany, A. A. García-Granada, *Int. Commun. Heat Mass Transfer* **2017**, *87*, 1.
- [22] L. Zhang, G. Zhao, G. Wang, G. Dong, H. Wu, *Int. J. Heat Mass Transfer* **2017**, *104*, 1246.
- [23] A. Kožušniková, P. Konecny, E. Plevova, L. Králová, *Procedia Eng.* **2017**, *191*, 426.
- [24] W. R. Wawersik, C. Fairhurst, *Int. J. Rock Mech. Mining Sci.* **1970**, *7*, 561.
- [25] F. W. J. Olver, D. W. Lozier, R. F. Boisvert, W. Charles, *Clark: NIST Handbook of Mathematical Functions*, Cambridge University Press, Cambridge **2010**.

How to cite this article: B. Zink, J. G. Kovács, *Polym. Eng. Sci.* **2022**, *62*(4), 1137. <https://doi.org/10.1002/pen.25912>